

Petrology and Geochemistry of Early Cambrian Volcanic Rocks Hosting the Kiruna-type Iron Ore in Anomaly 10 of Sechahun, Central Iran

A. Eslamizadeh*

Department of Geology, Faculty of Sciences, Islamic Azad University, Bafgh Branch, Islamic Republic of Iran

Received: 14 May 2016 / Revised: 9 August 2016 / Accepted: 17 September 2016

Abstract

Early Cambrian volcanic rocks of the Posht-e Badam tectonic block in Central Iran which is hydrothermally altered to green color rocks, hosts the Kiruna-type Iron Oxide-Apatite (IOA) mineralization in Anomaly 10 of Sechahun deposit. Geochemically, these volcanic rocks are classified as high-potassium calc-alkaline and mainly consist of rhyolite and trachyandesite. These rocks are important for hosting the REE-bearing apatite-iron oxide ores. The rhyolitic tuffs with a likely common origin are associated with the volcanic rocks. In this research, a selection of samples from Anomaly 10 of Sechahun has been studied with respect to their geochemistry and petrography with a special focus on REE-bearing phases. The bulk geochemistry of the rock units was analyzed using (ICP-OES) and (ICP-MS) methods. The ore samples were studied using ore microscopy and scanning electron microscopy with the energy-dispersive X-ray spectroscopy (SEM-EDS) techniques. The results indicated that mineralization has occurred by magmatic differentiation, forming magnetite, hematite, and apatite, followed by hydrothermal reworking, forming minerals such as hematite ± actinolite. Dendritic forms of magnetite, and apatite are common in the area. Apatite grains with monazite inclusions are generally enriched in LREE. The similar distribution of trace elements in various types of volcanic rocks in Anomaly 10 indicates a co-genetic origin and possible petrogenetic relation of these rocks. The whole rocks have been derived from differentiation of a single magmatic source. This magma with a probable melasyenitic initial composition erupted in a rifting tectonic environment and experienced some partial melting of the crust.

Keywords: Petrology; Geochemistry; Volcanic rocks; IOA-type; Sechahun.

Introduction

The Bafq-Posht-e-Badam metallogenic zone at the eastern part of Central Iran is the host of main iron

deposits (IOA-type) from Neoproterozoic-Lower Cambrian [1]. The iron deposits commonly formed due to multistage interactions of hydrothermal-magmatic processes within the Early Cambrian volcano-

* Corresponding author: Tel: +983532436870; Fax: +983532437070; Email: meslamizadeh@bafgh-iau.ac.ir

sedimentary sequence [2].

These deposits are commonly classified as IOA or Kiruna iron-apatite deposits that are usually associated with calc-alkaline volcanic rocks and Na-K-Ca (Mg)-Fe-P (REE) alteration on a deposit- to regional-scale [3]. They are up to 2 wt.% enriched in LREE but altered apatites are strongly depleted in these elements [4]. The apatite minerals in Sechahun like other iron ore deposits in the Bafq district are (REE)-U-P fluorapatite associated with magnetite, also fluorapatite is the main gangue in most of these deposits in the area [5, 6]. The study area to be considered as a section of Sechahun, is representing an IOA deposit in the Bafq district. The Sechahun iron mine consists of two separate ore bodies known as anomalies 10, and 11 with different geochemical characteristics. The iron deposits are chronologically hosted in upper Proterozoic-lower Cambrian volcano-plutonic rocks associated with a widespread phase of Na-metasomatism, economically, resulting in enrichment of the host rocks in REE bearing mineral phases [7]. The IOA or Kiruna-type deposits in Bafq District are associated with calc-alkaline volcanic rocks and have no relation with copper-gold deposits [3, 8]. The Bafq district iron ores are potentially of a great interest, especially because of continued interest in IOA and IOCG ore types. Thus this area has been the subject of a lot of academic literatures and researchers [9,10,11,12,13,14,15,16,17,18, 19, 20].

Some geologists believe this group of iron ore deposits has been formed directly from magma filling volcanic diatremes or flowing as lavas [7, 10] while others suggest metasomatic replacement of pre-existing rocks, charged with iron leached from cooling the felsic plutons [12]. The later researchers such as Moore and Modabberi, 2003 [21], suggested that most deposits in the Bafq mining district formed by separation of an iron oxide melt. Euhedral magnetite crystals in the area formed as open-space filling veins in both brecciated host and the wall rocks. In addition, the secondary magnetite has occurred as disseminated grains and veins in the altered brecciated host rocks and has the same composition as magnetite in massive lenses. Thus, like the El-Laco iron deposits in northern Chile [22], this feature along with the chemical fingerprint of magnetite, supports the influence of metasomatic replacement, followed by hydrothermal reworking in Sechahun rather than separation of an iron oxide-rich melt. Using chemical analysis of magnetite to constrain genesis of the IOA type Chadormalu magnetite-apatite deposit, as a major deposit in the Bafq district [23], also shows that various magnetite generations might be resulted of an ore-forming fluid that was initially magmatic-hydrothermal and evolved to moderate brine-dominated

meteoric water. The ore bodies in Sechahun consist of semi-massive ilmenite-rich magnetite, and coarse REE-rich fluorapatite, that based on U-Pb LA-ICPMS aging, are formed at 510 ± 8 Ma. [17, 11, 18, 5]. In general, the iron oxide-apatite deposits in the eastern Central Iran occurred in felsic volcanic rocks, tuffs and volcano-sedimentary sequences of Early Cambrian age [3]. The area has experienced crustal extension associated with an intercontinental rifting [10]. According to Torab and Lehmann, 2007 [24] and Torab, 2008 [18], the geological setting of the area is related to rifted continental margins (back arcs) and intercontinental rifts (anorogenic) in a subaerial to shallow marine basin sequence followed by volcano-plutonic activities. This study represents new geologic and geochemical data of volcanic rocks and related Fe-mineralization in Sechahun iron oxide-apatite deposit. It also provides an understanding of petrology and petrogenesis of the rocks and minerals in this area. Textural and compositional data are presented for distinctive types of volcanic rocks as the host of iron ore in Sechahun, to describe their relation and different mineralization models.

Materials and Methods

Geology and Analytical Techniques

Sechahun iron mine is situated on the east-west trending magnetic lineament that connects it to other iron ore deposits of the Bafq mining district. Anomaly 10 of Sechahun, characterized by three short black hills that is occurred in a relatively high-level plain in Sechahun area, about 45 km northeast of the Bafq City. The coordinates are $31^{\circ} 53' N$, and $55^{\circ} 41' E$. The lithology consists mainly of agglomerate, tuff and volcanic rocks (rhyolite and trachyandesite) that formed a folded anticlinal. There are extensive dislocations with a break in continuity of north-western and north-eastern directions. Composite-dislocated complex of sedimentary-volcanogenic formation of Early Cambrian takes part in the geological structure of the Sechahun mining area. The sedimentary rocks are black and gray limestone with intercalations of argillaceous sandstone and brown dolomite. The whole rocks at Anomaly 10 of Sechahun are covered by 2-15 meters of Tertiary conglomerate, sandstone, and schist, beneath Quaternary alluvial sediments. The intrusive-subvolcanic gabbro-syenite and magnetite mineralization are genetically associated with together, exclusive in this area. Gabbro, gabbro-diorites, diorites and granodiorites are rarely present but syenite and granite occurred widely among the rocks complex considerably far from the study area.



Figure 1. A view of Early Cambrian volcanic rocks enclosing the green rocks and ore-body of magnetite-apatite in the mining pit of Sechahun (Anomaly 10).

The ore-bodies are lenticular-layer shaped and chiefly composed of rich non-oxidized magnetite ores that occurred at the border of the volcanic and sedimentary rocks (Fig. 1).

The iron ore-bodies are mainly rich in magnetite. However, the low-grade iron ore with a high apatite content is found as well. Magnetite occurs as massive, lava flow, sill, dike, and pyroclastic forms. Other ore types are magnetite, magnetite-hematite, magnetite-apatite, pyrite-magnetite, and magnetite-silicate. The broad-scale hydrothermal alteration rocks as massive bodies of green rocks are associated with the magnetite-apatite deposit or as actinolite-rich veins are cutting through volcanic rocks. The iron mineralization has occurred mainly along cross cutting faults on the flanks of an anticline actinolite rich alteration zone.

Field work included delineating the volcanic rocks, actinolite-rich metasomatites rocks and iron ore contacts. The rock samples were taken over some profiles across the ore bodies and host rocks. Twenty-five samples, resulting in the detection of five minerals, namely magnetite, apatite and magnetite + hematite + apatite was collected from the ore body's outcrop in Anomaly 10 of Sechahun. The selected iron ores are representing by magnetite and hematite + magnetite varieties (Table 2, sample MA7 and MA8). The sulphide minerals are represented by pyrite, and less frequently by chalcopyrite (Fig. 4a). By its chemical composition, apatite is attributed to fluorapatite. The grain and aggregate of this mineral have irregular form and usually dispersed in ores (Fig. 4b). The dimension of apatite inclusions is mainly 0.02-0.2 mm. Thus, it was allowed to remove by magnetic separation from a considerable part of apatite. The grains of apatite with fluorapatite composition as mentioned by Daliran et al., 2007 [14], contain the idiomorphic REE-bearing

monazite inclusions. Multiple structures of intergrowth are characteristic of ores due to presence of titanium. They are formed dissociation structures of solid solution of ilmenite in magnetite and myrmekitic texture of sphe with ilmenite and rutile. Selected samples of volcanic rocks were analyzed using inductively coupled plasma optical emission spectrometry (ICP-OES) for major and trace element concentration (Perkin Elmer Optima 7300DV) and X-ray fluorescence (table 1) at the Zarazma laboratory in Tehran, Iran. The rare-earth elements and Th-U concentration in apatite, magnetite and magnetite-hematite + apatite was analyzed by ICP-MS (Perkin Elmer Nixon 300Q) at the same laboratory (table 2). Monazite based on the Scanning Electron Microscope (SEM), is the main REE-bearing mineral that occurred as inclusions in apatite (Fig. 4d). The Backscattered Electron (BSE) image of a thin-polish magnetite-apatite sample is provided by Iranian Mineral Processing Research Center.

Petrography and Mineralogy

Volcanic rocks are acidic to intermediate composition with the SiO₂ content ranging from 56 to 71 percent, including rhyolite, rhyodacite, trachyte, and trachyandesite. Their colors are white, pinkish or light gray. The rhyolitic group with aphanitic to porphyritic textures are predominate and usually contain phenocrysts of quartz, and plagioclase. The matrix is dominated by quartz, and feldspars. The primary feldspars have transformed to chessboard albite (Fig. 2a and b). Hydrothermal alteration has partly replaced feldspars by kaolinite, sericite, and calcite. There are massive and non-welded tuffs, which show the similar composition with the rhyolitic rocks, that may indicate a common origin of formation. The andesitic rocks are the most abundant after acidic and rhyolitic rocks.

Formation of andesite is dominated by mixing of iron and magnesium rich (mafic) magmas and silicate rich (felsic) magmas [25]. Basaltic andesite rocks in the Anomaly 10 of Sechahun have a fine-grained porphyritic texture dominated by phenocrysts of

plagioclase, pyroxene and hornblende (Fig. 2c and d). Irregular crystals of sphene are abundant in the completely altered rocks. Hydrothermal alteration of the volcanic host rocks led to form the secondary minerals such as tremolite- actinolite, epidote, and chlorite. The

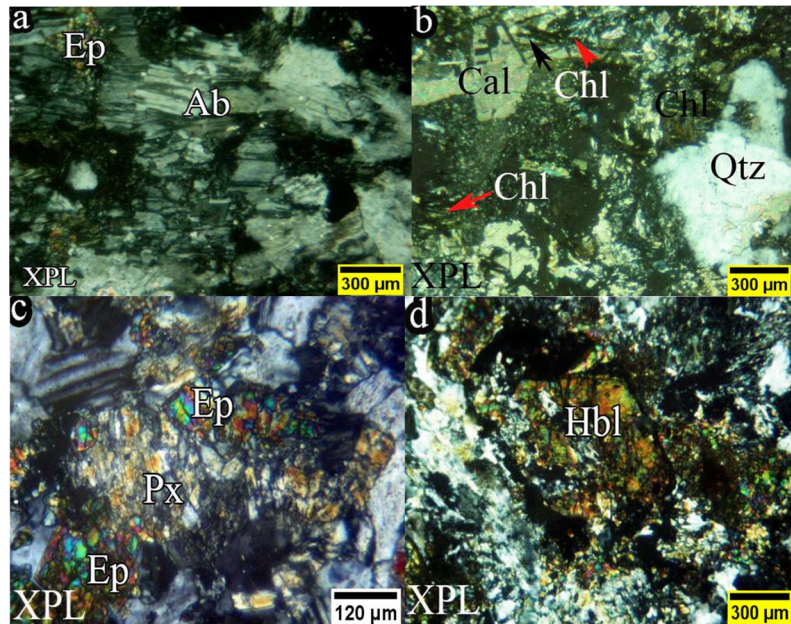


Figure 2. (a,b) Microphotographs of porphyritic rhyolite with albite and quartz phenocrysts. (C,d) Microphotographs of basaltic andesite rocks with large visible pyroxene and hornblende phenocrysts.

Abbreviations: Ab-albite Qtz-quartz Chl-chlorite Ep-epidote Hb-hornblende Px-pyroxene

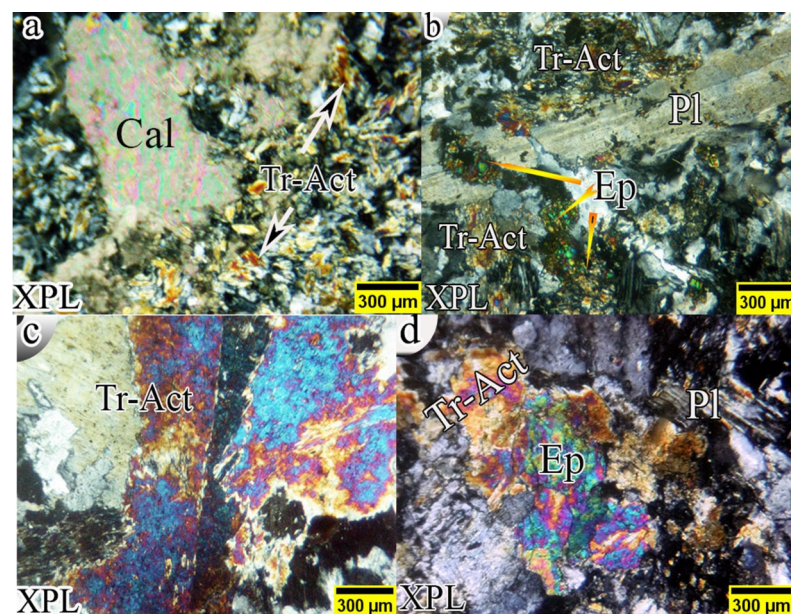


Figure 3. (a-d) Microphotographs of the green rocks including hydrous altered types of the volcanic rocks composed of epidote and tremolite- actinolite. Abbreviations: Cal-calcite, Tr-Act: tremolite- actinolite, Pl-plagioclase, Ep-epidote.

'green rocks' environment is comparable to propylitic alteration characterized by hydrothermal minerals such as actinolite, albite, epidote, calcite and chlorite. This alteration typically represents the most distal, weakest imprint of hydrothermal activity, and such alteration may develop in a wide range of ore deposit systems [26]. The representative microphotographs in figure 3 (a-d), show some petrographic aspects of the green rocks commonly having an abundance of green minerals. The associated alterations include

carbonatization, silicification and replacement of primary minerals to epidote and tremolite- actinolite by Ca-Mg-Fe metasomatism.

Massive and brecciated green rocks are usually found at contacts of iron ore bodies, and rhyolitic rocks. Generally, in the Bafq mining district, alkali-metasomatism as amphibolytization and albitization has paragenetically occurred around the iron ore deposits [7]. Tremolite and actinolite as long prismatic crystals are widely developed in the spaces between magnetite

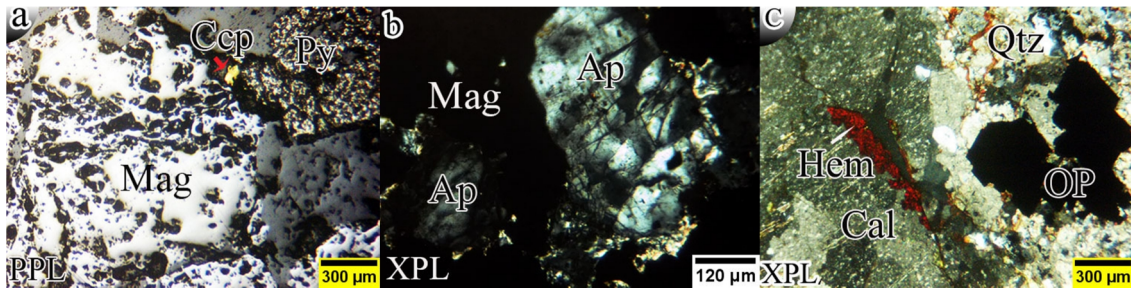


Figure 4. a. Photomicrographs of magnetite ore with pyrite, and chalcopyrite in polished section. b. Magnetite, and apatite in thin section c. Quartz- carbonate and Fe-oxide alteration along the joints, and fractures. Abbreviations: Mag-magnetite, Py-pyrite, Ccp-chalcopyrite, Ap-apatite, Hm-hematite, Qtz-quartz, Cal-calcite, Op-opaque.

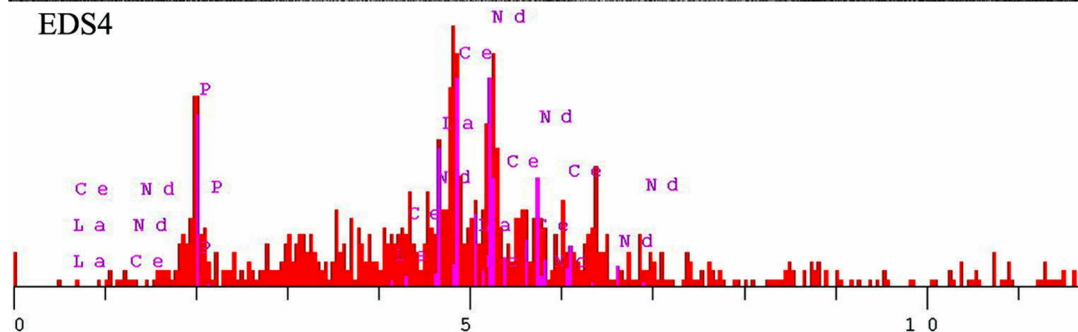
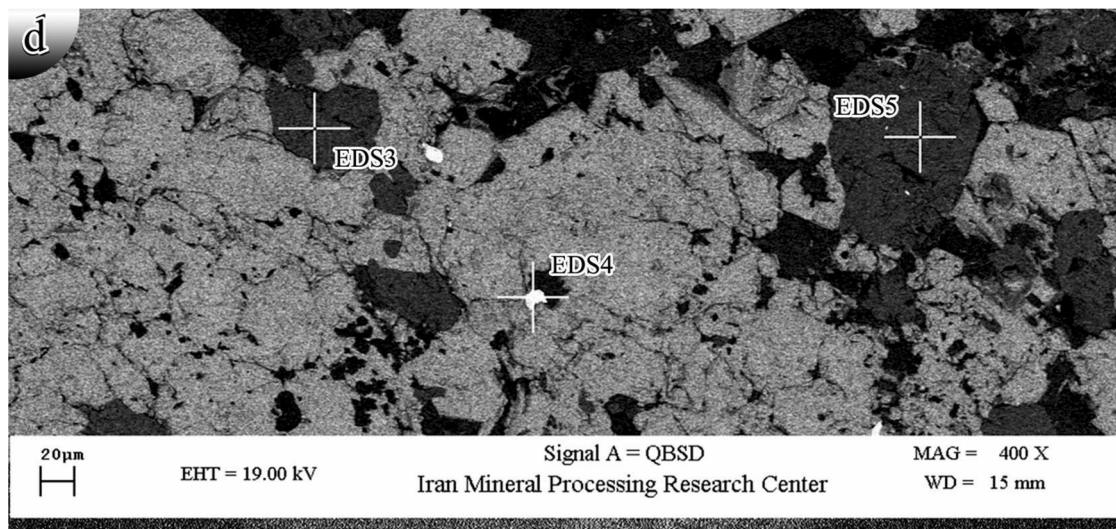


Figure 4. d. Backscattered electron (BSE) images of apatite from the Anomaly 10 of Sechahun white monazite inclusions rich in Ce, La, Nd in a dark apatite phase.

grains in Anomaly 10 of Sechahun and can be seen with the unaided eye. Primary magnetite ranges from a medium grained to coarse- grained crystals. These crystals similar to some other magnetite ore deposits in the Bafq region like Choghart [21] and Zaghia [27], commonly show intimate intergrowths with sharp 120° contacts, typical for crystallization from a melt. Magnetite also presents as banded, brecciated, and impregnated ore (Fig. 4a-b). Ilmenite, and titanite as evidence of the extra TiO_2 content are identified under the microscope. The primary hematite is rarely seen in an ore body associated with magnetite and pyrite in some mineralized veins. Martitization is a widespread event, and the earliest magnetite has partly replaced by martite. It begins at grain boundaries and fractures of magnetite indicating the role of hydrothermal overprint, and metasomatic rock-replacement interactions besides weathering [18]. The alteration assemblages in volcanic rocks associated with the iron ore deposits show a diversity from sodic (albitization) to potassic alteration (K-feldspar, and sericite). The silicic alteration consists of quartz- sericite assemblage is widespread. Actinolite is widely distributed in the hydrothermally altered volcanic rocks associated with chlorite, and epidote. The volcanic rocks have been extremely altered, especially adjust the mineralization zone as identification of the original rocks is very difficult. The mineralization of magnetite, hematite, and apatite is followed by creation hydrothermal minerals such as hematite \pm actinolite. The impregnated phosphate presents in shear zones, and massive iron ore bodies. The late stages of mineralization are characterized by quartz- carbonate alteration along the joints, and fractures (Fig. 4c). Goethite and hydrogoethite are

developed mainly in the subsurface zone. Apatite also exists as an idiomorphous inclusion within the magnetite that occurs as a granular interstitial mass in oxidized zones.

Monazite inclusions in apatite are rich in Ce, La, Nd (Fig. 4d). Fluorapatite is a common mineral and is associated with some accessory REE-bearing minerals such as monazite, allanite, parasite and xenotime. Monazite crystallized as inclusions inside apatite besides forming relatively large individual crystals [18]. As a result, the paragenetic minerals of the iron ore in Anomaly 10 of Sechahun include pyroxene, apatite (fluorapatite), pyrite, magnetite, biotite, alkali feldspar (orthoclase and microcline), quartz, albite, ilmenite, dolomite, calcite. The post magmatic phases are characterized by minerals such as talc, chlorite, tremolite, epidote, sericite, chalcopyrite and calcite. Martite, rutile, goethite and quartz-chalcedony are developed during the secondary alteration.

Results and Discussion

Geochemistry

1. Major elements

The analysis results of major, trace, and rare- earth elements of the particular fresh volcanic rocks are shown in tables 1 and 2. Geochemical classification of the studied rocks ($SiO_2 \approx 56-71$ wt.%) using total alkali versus silica (TAS) diagram [28] indicates that rhyolitic rocks plot in the field of sub-alkaline but trachyte samples locate on the field of alkaline (Fig. 5). It is likely related to an extensive Na-Ca metasomatic alteration, and albitization that are obvious in the microscopic study. Both Na_2O and K_2O behave

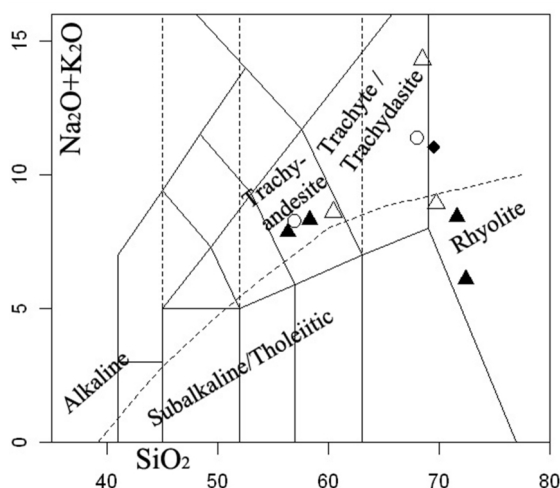


Figure 5. Total alkali- silica diagram of the volcanic rocks (Le Bas et al. 1986) [28]. The dividing line between alkaline and sub-alkaline fields is after Irvin and Baragar, 1971 [29].

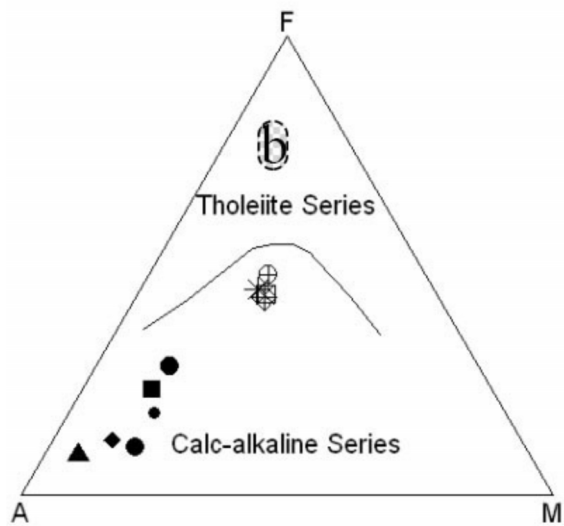
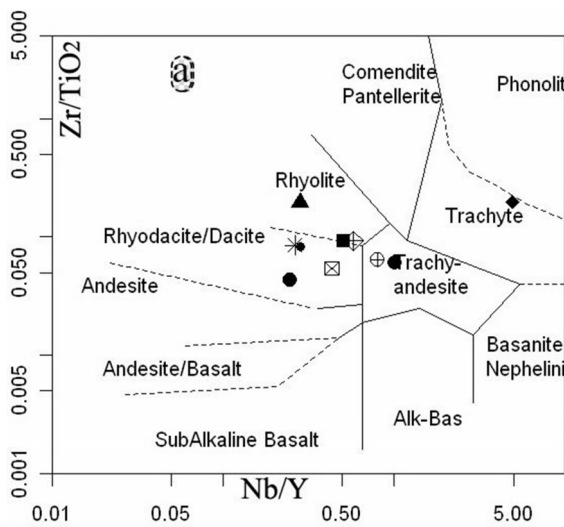


Figure 6. a. Composition of rock samples in the discriminant diagram of Zr/TiO_2 versus Nb/Y Winchester and Floyd, 1977 [30]. b. The AFM diagram of Irvin and Baragar, 1971 [29].

essentially incompatible by the progressive fractionation stages.

Due to extensive alteration, the analyzed samples are plotted on the discrimination diagram of Winchester and Floyd, 1977 [30] that is widely used for discriminating of the altered volcanic rocks (Fig. 6a). In the following diagrams, the more felsic rocks are located on the "Rhyodacite-dacite" compositional field and only a few sample plot within the field of "Rhyolite," "Trachy-andesite," and "Trachyte." All lava samples place on the calc-alkaline field of Irvin and Baragar, 1971 [29] on the AFM ($Na_2O + K_2O - FeO - MgO$) diagram (Fig. 6b).

Based on Co-Th plot from Hastie et al, 2007 [31] that is shown in Fig.7, most samples exhibit apparent strong

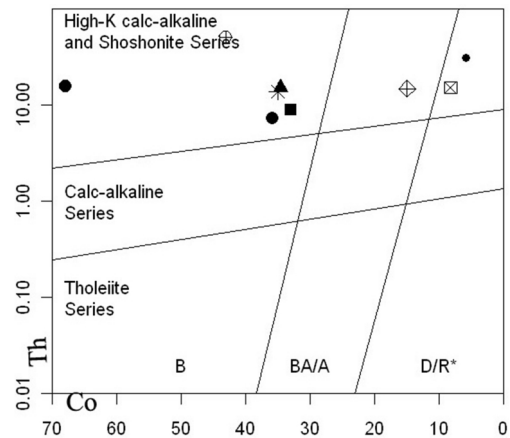


Figure 7. The Co-Th plot from Hastie et al, 2007 [31].

high-potassium calc-alkaline affinity, and only a few sample plot on the shoshonitic persodic (Na_2O/K_2O ratio > 1). According to the field works and geochemical evidence, it is likely related to an earlier metasomatized mafic thick lower-crustal source that enriched in alkalis under CO_2 -bearing partial melting due to raising the asthenosphere up welling beneath an incomplete rift [32].

By using Harker diagrams, the systematic variation of the major and trace elements in the volcanic host rocks has studied in order to understand the petrogenesis and quality of the fractional crystallization. However, use of some diagrams applied to analysis of the volcanic rocks is difficult due to lack of data for creation of the discriminant lines between rock series. There is a gap between 60-65 wt.% SiO_2 zones due to lack of samples with 60-65% SiO_2 content. The relevant positions are provided for sufficient points to enable accurate plotting of the diagrams.

The CaO , MgO and FeO versus SiO_2 show a relatively continuous decreasing trend with silica increasing, confirms the role of plagioclase and magnetite differentiation and ferromagnesian phases such as olivine and pyroxene as major fractionating phases in magmatic evolution (Fig. 8).

The decreasing trend of FeO to silica compared to MgO trend, shows somewhat discontinuity. Fe has bigger ionic radius and less compatibility than Mg, and both can enter the solid solution ferromagnesian phases. The Fe-rich end members of these series have a lower crystallization point. So at the beginning of crystallization, Fe content is less than Mg and its decreasing trend versus SiO_2 can't be as prominent as Mg. On the silica variation diagrams, SiO_2 , Al_2O_3 , Na_2O and K_2O contents of volcanic rocks somewhat increase and CaO , MgO and FeO , declines with increasing

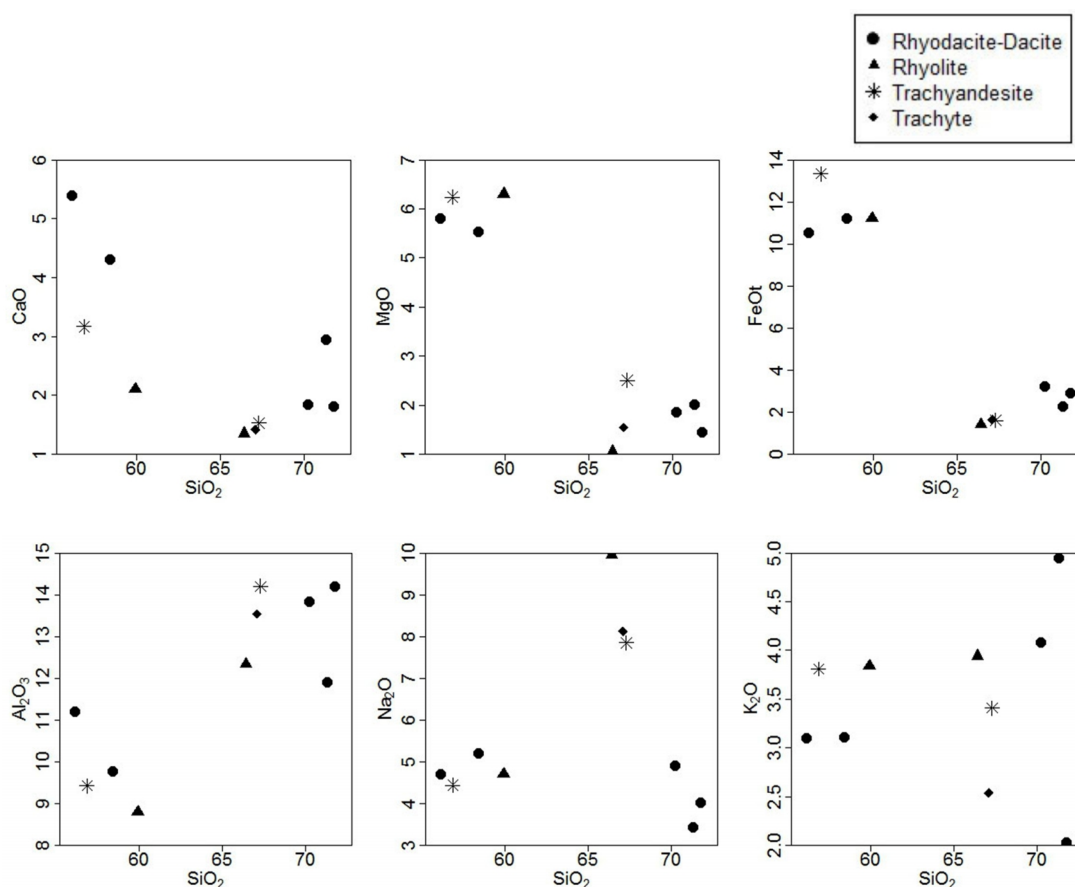


Figure 8. CaO, MgO, and FeOt versus wt.% SiO₂, and silica variation diagrams of Al₂O₃, Na₂O and K₂O.

differentiation from trachyandesite to rhyolite, but samples are often scattered due to intense alteration. The rhyolitic rocks, that contain more than 20% phenocryst of alkali feldspar have a higher percentage of Al₂O₃.

K₂O and NaO show curvilinear trends and scatter with increasing SiO₂. However, such scattering is presumably attributed to crustal contamination processes but K as a Large-Ion Lithophile (LIL) element with high ionic radius, has most incompatibility and concentrates in more acidic rocks. In rhyolite and rhyodacitic rocks, K₂O shows a rising trend with SiO₂ increasing but scatters in trachyte and trachy-andesitic rocks. Due to a smaller ionic radius of Na, it is more compatible than K, and shows a positive correlation with the SiO₂ and K₂O in intermediate and acidic rocks. The Na abundance in sodic feldspars and albite as the secondary minerals in the studied volcanic rocks led to the formation of rock type collection without having a continuous trend with increasing the SiO₂.

2. Trace elements

The composition of trace elements in studied volcanic rocks (table 1 and Fig. 9a), normalized and compared with the average elementary composition of the crust (Weaver et al., 1984) [33], show the same pattern, origin and genetic similarities. All volcanic rocks are enriched in La, U, and relatively in Y, depleted in Ba, Ti, P, and Nb. In order to study depletion and enrichment of trace elements in various types of the volcanic rocks, they were compared with the average elementary composition of the crust (Weaver et al., 1984) [33], (Fig. 9 b-d). Yttrium as an HREE shows relatively enrichment in all rock's types. The Y amount in trachyandesitic rocks is about 19 ppm and reaches to 65 ppm in rhyodacite. According to Gill, 2012 [34], Y with greater than 15 ppm belongs to andesitic rocks that erupted in a crustal area with more than 30 kilometers thickness. The Zr amount of the rocks compare to the earth crust shows a depletion. Zircon as an immobile element is widely controlled by the geochemistry of its resource and indicates a crustal origin [35].

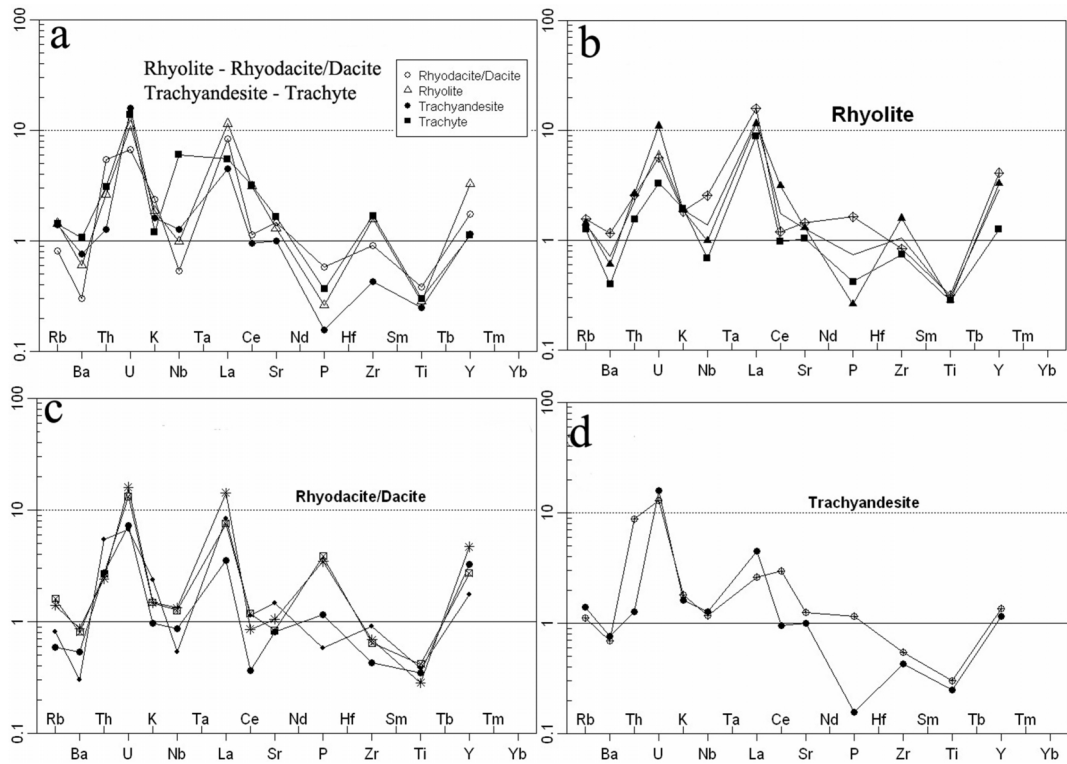


Figure 9. (a-d) The distributions of normalized trace element composition in volcanic rocks compared to average elementary composition of the crust (normalized values from Weaver et al., 1984 [33]).

The fractionation of magnetite, ilmenite, and apatite during early magmatic stages is the reason for P and Ti reduction in the volcanic rocks. The negative Ba anomaly in rhyodacitic rocks is probably related to Ca be substituting in primary plagioclase feldspars, and segregation from magma. However, the greater crystal lattice elasticity of albite compared to anorthite is a

reason for the preference absorption of Ba in albite than anorthite [36] but albite in the studied volcanic rocks created after albitization of the primary feldspars. U and Th as High-Field Strength (HFS) elements have strong enrichment in all types of volcanic rocks in the study area (Table 1). Unlike of LIL elements, the HFS elements remain stable during the alteration process.

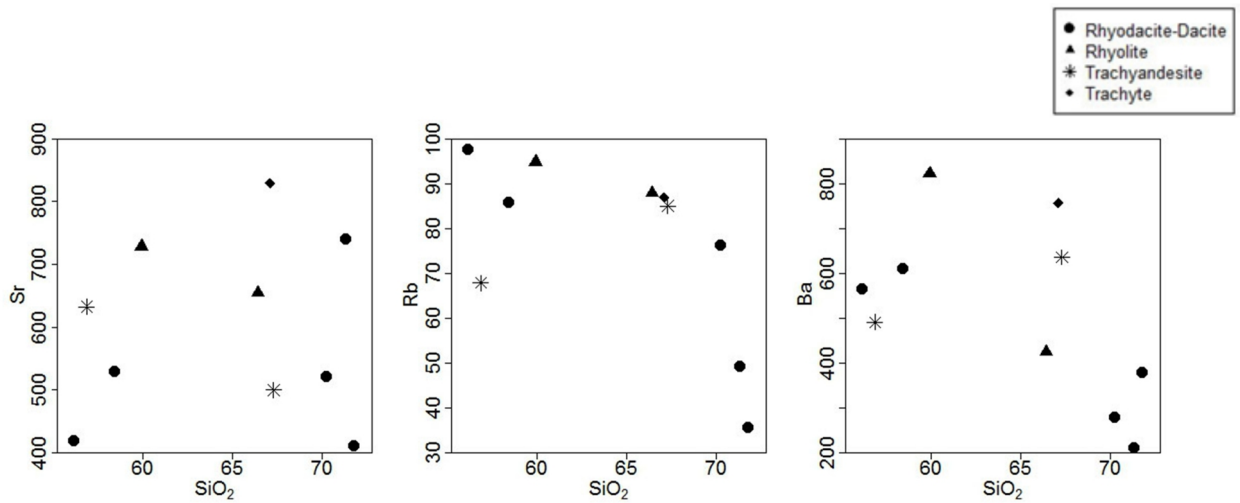


Figure 10. The silica variation diagrams Sr, Rb and Ba.

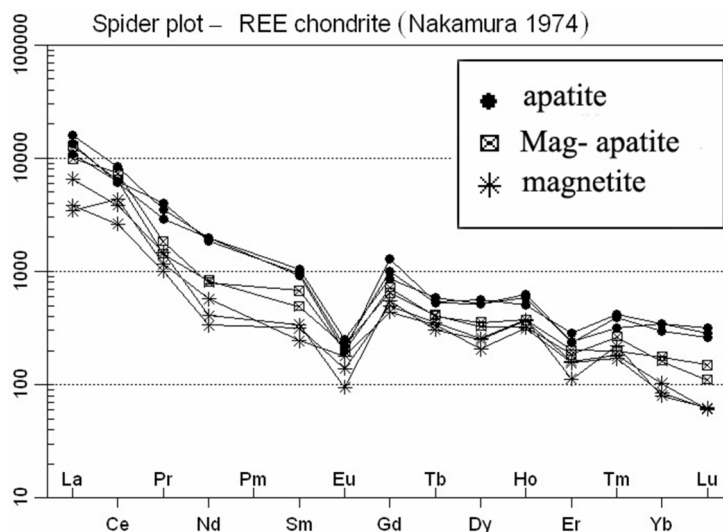


Figure 11. The chondrite normalized REE diagram of apatite, magnetite-apatite, and magnetite samples.

Thorium has a range of 7 to 50 ppm in trachyandesitic rocks (Table 1). Th enrichment is related to monazite cores that exist as nucleus inclusions within apatite or individual crystals out of apatite.

Silica variation diagrams of Sr, Rb and Ba are illustrated in Fig. 10. The amount of strontium varies from 411 to 829 ppm in trachytic rocks. Ascending and descending trends in this graph are probably related to the changing amount of feldspar and existence of albite phenocryst.

Both Sr and K are in Low Field Strength (SFS) elements and due to increasing potassium, Sr increases in andesite. It has a positive correlation with SiO_2 only in the low-potassium andesite but remains constant or decline in high-potassium andesite. Like Sr, Ba shows a wavy pattern with increasing silica when it reaches a climax of concentration around 65 wt.% silica, then start to decline with the silica increasing. The Ba concentration decreases from 821 to 281 ppm with increasing the silica in rhyolitic rocks of Anomaly 10 of Sechahun, but it is steadier in the trachyte and rhyodacite rocks.

El-Bialy, 2010 [35] also indicated this Ba behavior in Dokhan volcanic, Central Eastern Desert of Egypt. Finally, a positive correlation between K_2O and Ba documented by Gill, 2012 [34], and according to this statement, Ba can substitute for potassium in silicate or for calcium in plagioclase. Therefore, such trends on the variation diagrams of studied volcanic rocks can be assumed by changing the amount of calcic plagioclase and sodic-potassic feldspars. Rb usually, substitute for potassium in silicate structures, so it has a positive correlation with K_2O . The Rb amount is in the range of

35 ppm in dacite to 94 ppm in rhyolite. The variety of K_2O in these rocks causes the rising and descending trend. In general, the influence of linear trends on the variation Harker diagrams in the volcanic rocks, indicate the fractional crystallization and differentiation in magmatic evolution. The effect of an alteration process most probably has caused the wavy and scatter patterns. The higher ratio of Ba/Nb (32.7) and lower values of Nb/U (1.2), Ba/La (2.3), U/Th (0.73) indicated that the source may have been modified by some melts derived from the relatively incompatible element-rich sediments [37]. Furthermore, the higher La (73.6 – 443.6 ppm) contents reflect that the high-potassium magmas may have been produced by small degrees of partial melting in a metasomatized source.

3. Rare earth elements

In order to study of the REEs quantity and distribution in the study area, the ICP-MS analysis result of some iron ore samples, rich in apatite, including magnetite, apatite, and hematite ores used for this research (Table 2). All results normalized with chondrite values from McDonough and Sun 1995, [38]. As presents in Fig. 11, the patterns of all three groups are the same but apatite has more REE content than other minerals.

Unlike apatite, the minerals of magnetite, and hematite are unsuitable collectors for REEs. Therefore, the similarity between magnetite and apatite patterns with consideration of hydrothermal evidence in the area shows that their origin cannot be purely a magmatic source [18]. Another proof that shares the answer is due to existence of monazite as a common REE bearing

Table 1. Major element abundances (Wt.%) by ICP-OES and trace elements (ppm) by XRF

| Sample | AS01 | AS02 | AS03 | AS04 | AS05 | AS06 | AS07 | AS08 | AS09 | AS10 |
|--------------------------------|--------|--------|--------|--------|-------|--------|-------|-------|--------|--------|
| Description | Ta | Rh | Tr | RhD | RhD | RhD | RhD | RhD | Rh | Ta |
| | | | | | Wt. % | | | | | |
| SiO ₂ | 67.31 | 66.44 | 67.1 | 71.81 | 71.34 | 70.27 | 56.1 | 58.41 | 59.9 | 56.84 |
| Al ₂ O ₃ | 14.2 | 12.34 | 13.56 | 14.2 | 11.95 | 13.84 | 11.2 | 9.78 | 8.8 | 9.43 |
| FeO _t | 1.61 | 1.42 | 1.66 | 2.93 | 2.27 | 3.22 | 10.54 | 11.21 | 11.2 | 13.34 |
| CaO | 1.53 | 1.35 | 1.42 | 1.81 | 2.95 | 1.84 | 5.4 | 4.31 | 2.1 | 3.17 |
| Na ₂ O | 7.85 | 9.95 | 8.12 | 4.02 | 3.43 | 4.91 | 4.71 | 5.21 | 4.7 | 4.44 |
| K ₂ O | 3.41 | 3.94 | 2.54 | 2.03 | 4.95 | 4.08 | 3.1 | 3.11 | 3.84 | 3.81 |
| MgO | 2.51 | 1.05 | 1.55 | 1.45 | 2.02 | 1.85 | 5.8 | 5.54 | 6.3 | 6.24 |
| TiO ₂ | 0.15 | 0.17 | 0.18 | 0.21 | 0.23 | 0.17 | 0.25 | 0.17 | 0.19 | 0.18 |
| MnO | 0.04 | 0.05 | 0.06 | 0.07 | 0.06 | 0.05 | 0.05 | 0.09 | 0.07 | 0.11 |
| P ₂ O ₅ | 0.03 | 0.05 | 0.07 | 0.22 | 0.11 | 0.08 | 0.73 | 0.66 | 0.31 | 0.22 |
| S | 0.1 | 0.59 | 1.02 | 0.52 | 0.32 | 0.14 | 0.13 | 0.23 | 1.27 | 0.42 |
| L.O.I | 2.10 | 2.71 | 3.86 | 1.64 | 1.22 | 1.01 | 2.1 | 1.56 | 1.92 | 1.84 |
| Total | 100.75 | 100.06 | 101.12 | 100.91 | 100.8 | 101.46 | 100.1 | 100.2 | 100.06 | 100.04 |
| | | | | | ppm | | | | | |
| Cl | 36.7 | 28.4 | 27.7 | 67 | 35.7 | 44.8 | 57.4 | 74 | 76 | 87 |
| Ba | 535.8 | 424.5 | 757.3 | 380.3 | 212.9 | 280.5 | 565.9 | 612.8 | 821.7 | 491.1 |
| Sr | 500.3 | 654.7 | 829 | 411.9 | 741.3 | 521.7 | 420.5 | 530.6 | 728.3 | 632.7 |
| Cu | 15.2 | 52.3 | 45.3 | 44.1 | 12.2 | 13.54 | 17.65 | 13.4 | 13 | 14.31 |
| Zn | 154.5 | 194.3 | 170.9 | 109.5 | 100.7 | 90.7 | 61.2 | 90.3 | 70.3 | 54.4 |
| Pb | 28.2 | 13.5 | 16.3 | 14 | 6.5 | 5 | 5.7 | 6.3 | 4.7 | 9.3 |
| Ni | 12.2 | 13.8 | 33.8 | 31.5 | 17.4 | 30.6 | 41.9 | 15.2 | 14.9 | 17.7 |
| Cr | 12 | 44.1 | 80.3 | 23.9 | 46.9 | 43.7 | 67.3 | 34.7 | 55.9 | 61.8 |
| V | 27.3 | 227 | 236.3 | 205.5 | 65 | 52.2 | 82 | 37.6 | 153 | 148.4 |
| Ce | 54.3 | 178.54 | 181.36 | 20.84 | 64.31 | 55.67 | 67.35 | 48.7 | 68.33 | 170.31 |
| La | 126.2 | 323 | 154.3 | 98.5 | 235.5 | 248.5 | 211.3 | 398.3 | 443.6 | 73.6 |
| W | 1.5 | 3.7 | 1.7 | 4.1 | 7.5 | 4.3 | 4.6 | 3.8 | 7.9 | 8.3 |
| Zr | 90.6 | 331.7 | 354.7 | 90 | 190.5 | 156.3 | 135.8 | 144.6 | 175.9 | 114.8 |
| Y | 16.3 | 45.8 | 15.7 | 45.8 | 24.6 | 17.6 | 37.9 | 65.6 | 57.4 | 19 |
| Rb | 85 | 87.9 | 86.9 | 35.8 | 49.3 | 76.4 | 97.7 | 85.9 | 94.8 | 67.9 |
| Co | 35.8 | 34.6 | 76.4 | 67.9 | 5.8 | 33 | 8.3 | 35 | 15 | 43 |
| As | 12.7 | 5.7 | 6.2 | 0.13 | 3.7 | 5.9 | 4.3 | 4.3 | 4.6 | 4.3 |
| U | 20.5 | 14.3 | 18 | 9.4 | 8.7 | 4.3 | 17.3 | 20.8 | 7.3 | 16.9 |
| Th | 7.2 | 15 | 17.7 | 15.6 | 31.1 | 8.9 | 15.2 | 13.8 | 14.7 | 50 |
| Mo | 5.2 | 2.2 | 5.3 | 7.8 | 8.4 | 7 | 4 | 8.4 | 6.9 | 9.7 |
| Ga | 11.2 | 18.3 | 10.6 | 13.2 | 10.5 | 6.7 | 13.4 | 15.2 | 6.9 | 2.1 |
| Nb | 16.5 | 12.9 | 78.2 | 11.3 | 7 | 8.9 | 16.4 | 17.3 | 23.2 | 15.2 |

Abbreviation: Tr. Trachyandesite, Rh. Rhyolite, Tr. Trachyte, RhD. Rhyodacite-Dacite, Ta. Trachyandesite

mineral in free particles and to some degrees in mixed grains with magnetite [39]. It would be possible that some apatite, and magnetite minerals provided from the source rocks by hydrothermal solutions. Subsequently, hydrothermal fluids increased or reduced REE concentrations according to the apatite amounts. The steep decline and more or less steady patterns indicate LREE severe separation from HREE. It also shows HREE depletion and concentration of LREE in apatite. In the analyzed apatite samples, the $(La/Lu)_{en}$ ratio changes from 42.5 to 57.4 (table 2) indicating a high fractionation degree and the average ratio of $(La/Sm)_{en}$ is about 14.3 while the average ratio of $(Gd/Lu)_{en}$ is 3.7 conforming that the LREE fractionation is more than three times of HREE. The abnormal LREE increasing in

magnetite samples shows $(La/Lu)_{en}$ ratio of 110.5 (Table 2) that might occur by the existence of some inclusions. The severe fractionation LREE/HREE ratios of magnetite-hematite might be due to placing the microscopic REE-bearing minerals within the crystallographic lattice of magnetite by post-magmatic solutions. All samples show a distinct negative Eu anomaly on the chondrite normalized REE diagram. The Eu depletion is probably because of plagioclase removal from the source or later discarding by fractional crystallization in the magma chamber prior to emplacement [40]. Under the lower-oxygen fugacities Eu^{+2} substitutes by Ca^{+2} in plagioclase or magnetite structure and the higher degree of Eu fractionation separates it from other rare-earth elements [41]. It could

Table 2. REE and Th-U, concentration (ppm) in Anomaly 10 of Sechahun analyses by ICP-MS. (Magnetite, apatite and **magnetite –hematite + apatite)

| Sample | MA1 | MA2 | MA3 | MA4 | MA5 | MA6 | MA7 | MA8 | |
|-----------------|-------|---------|--------|----------|----------|----------|--------------|-------------|--------|
| Elements | Mag | Mag | Mag | Apatite | Apatite | Apatite | **Mag +He+Ap | Mag +He+ Ap | Ch* |
| La | 1135 | 1258 | 2162 | 5260 | 3570 | 4420 | 4250 | 3285 | 0.232 |
| Ce | 3750 | 2280 | 3320 | 7260 | 5450 | 5260 | 5550 | 6410 | 0.613 |
| Pr | 129.4 | 112.2 | 165.3 | 395 | 449 | 327.6 | 158.38 | 205.2 | 0.0928 |
| Nd | 358.2 | 211 | 254.7 | 1250 | 1170 | 1254 | 523.6 | 500.1 | 0.457 |
| Sm | 49.36 | 63.9 | 68.5 | 186 | 196 | 209.8 | 98.6 | 138.1 | 0.148 |
| Eu | 13.84 | 10.72 | 7.3 | 15.34 | 16.72 | 19.24 | 16.9 | 15.1 | 0.0563 |
| Gd | 121.2 | 136.9 | 151.4 | 356.2 | 278.4 | 239 | 180 | 197 | 0.199 |
| Tb | 15.8 | 16.59 | 14.3 | 25.2 | 24.8 | 27.6 | 19.4 | 18.9 | 0.0361 |
| Dy | 70.6 | 87.7 | 85.7 | 192.5 | 176.9 | 176.3 | 112 | 122 | 0.246 |
| Ho | 22.12 | 26.1 | 25.8 | 35.72 | 41.31 | 43.4 | 22.8 | 26.1 | 0.0546 |
| Er | 34.9 | 25.31 | 36.3 | 63.6 | 52.5 | 53.8 | 41.4 | 45.5 | 0.16 |
| Tm | 5.1 | 6.6 | 5.43 | 12.55 | 11.77 | 9.44 | 7.85 | 5.9 | |
| Yb | 18.7 | 17.6 | 22.7 | 75.6 | 65 | 75.3 | 35.53 | 38.52 | 0.161 |
| Lu | 2.08 | 2.11 | 2.05 | 9.6 | 8.8 | 10.8 | 3.72 | 5.05 | 0.0243 |
| Y | 767 | 30.9 | 11.2 | 1670 | 1560 | 1810 | 1540 | 1452 | |
| U | 6.4 | 8.84 | 3.25 | 9.62 | 12.2 | 12.1 | 8.4 | 9.1 | 0.704 |
| Th | 55.4 | 10.7 | 13.7 | 96.2 | 153 | 79.1 | 97.4 | 89.7 | 0.029 |
| Sc | <1 | <1 | <1 | 3 | <1 | 3 | 4 | 2 | |
| LREE | 5557 | 4072.72 | 6129.2 | 14722.54 | 11130.12 | 11729.64 | 10777.48 | 10750.5 | 1.7981 |
| HREE | 169.3 | 182.01 | 192.28 | 414.77 | 381.08 | 396.64 | 242.7 | 261.97 | 0.682 |
| LREE/HREE | 32.8 | 22.4 | 31.9 | 35.5 | 29.2 | 29.6 | 44.4 | 41.0 | 2.6 |
| (La/Lu)cn | 57.2 | 62.4 | 110.5 | 57.4 | 42.5 | 42.9 | 119.7 | 68.1 | |
| (La/Sm)cn | 14.6 | 12.5 | 20.1 | 18.0 | 11.6 | 13.4 | 27.5 | 15.2 | |
| (Gd/Lu)cn | 7.1 | 7.9 | 9.0 | 4.5 | 3.9 | 2.7 | 5.9 | 4.8 | |

* Chondrite values from McDonough and Sun, 1995 [38].

be a result of the fH₂O variations, during subcontinental lithosphere melting not by crystal fractionation processes from a host magma [40, 42].

As shown previously in Fig.4a, primary feldspars in the volcanic host rocks converted to albite during albitization. A portion of Eu-bearing elements fixed selectively in plagioclase structure, substituted for Ca that had already leached while other rare-earth elements mobilized out of the rocks towards hydrothermal systems and subsequently fixed in apatite structure of the magnetite-apatite ores.

According to Taylors and McLennan, 1995 [43], the REE distribution patterns depend on the bulk REE composition in parental magma. An intense LREE/HREE fractionation and large Eu depletion probably indicate a related alkaline parental magma erupted in a rifting environment [26]. Based on the previous models and a comparison of the results from petrological and geochemical evidence, all volcanic rocks and iron ore bodies in Anomaly 10 of Sechahun, are considered to produce from differentiation of a magma with a probable melasyenitic source in an intercontinental rift tectonic environment.

Conclusion

Based on petrographic results, the volcanic rocks are

mainly composed of rhyolite and rhyodacite along with trachyte, trachyandesite and basaltic andesite. The massive and non-welded rhyolitic tuffs nearby the volcanic rocks, likely have a common magmatic province with them. The hydrothermally altered volcanic rocks as huge bodies of green color rocks are hosts of the Kiruna-type Iron-Oxide-Apatite (IOA) deposits in Anomaly 10 of Sechahun. Apatites with monazite inclusion are rich in Ce, La, Nd, and their fractionation indexes of LREE are more than three times of HREE. The distribution model of REE in apatite is similar to magnetite with slightly lower values. This unusual similarity is due to crystalline structure of magnetite that is not a suitable collector for the REE, probably can be explained by the presence of monazite or other REE carrier minerals in free or mixed grains with magnetite. However, the hydrothermal fluids could increase or reduce the REE concentrations. All volcanic rocks are calc-alkaline, and their comparable trace element distribution indicates that these rocks have derived from the same source. The volcanic rocks are enriched in La, U and minor in Y. In contrast; they are fairly depleted in Ba, Ti, P and Nb. Depletion of Nb is most characteristic for magmatic evolution of the continental crust. The similarity of distribution patterns of magnetite and apatite shows that portion of apatite

and magnetite was generated from similar source rocks by hydrothermal activities. Subsequently, the hydrothermal fluids increased or reduced REE concentrations according to the apatite amounts. The fractionation of magnetite and ilmenite with apatite during early magmatic stages is the reason of reducing P and Ti in volcanic rocks. The incoherence of high value of U and the rock compositions, LREE enrichment and the negative Eu anomaly are indications of an open-system fractional crystallization and some partial melting, which most probably derived from differentiation of the magma related to an intercontinental rift tectonic environment.

The metasomatized volcanic rocks associated with magnetite- fluorapatite in Anomaly 10 of Sechahun likely created by the lower crust sourced alkaline low-degree partial melts and hydrothermal fluids that evolved to moderately brine-dominated meteoric water.

Acknowledgments

I would like to thank the anonymous reviewers for their careful reading and their many insightful comments and suggestions on the earlier version of the manuscript. The revisions reflect all reviewers' suggestions that resulted in a stronger manuscript. Although any errors are my own and should not tarnish the reputations of these esteemed persons.

References

1. Nabatian G., Rastad E., Neubauer F., Honarmand M. and Ghaderi M. Iron and Fe–Mn mineralization in Iran: implications for Tethyan metallogeny. *Aust. J. Earth. Sci.* **62** (2): 211-241 (2015).
2. Zaremotlagh S. and Hezarkhani A. A geochemical modeling to predict the different concentrations of REE and their hidden patterns using several supervised learning methods: Choghart iron deposit, bafq, Iran. *J. Geochem. Explor.* **165**: 35-48 (2016).
3. Stosch H.G., Romer R.L., Daliran F. and Rhede D. Uranium–lead ages of apatite from iron oxide ores of the Bafq District, East-Central Iran. *Miner. Deposita.* **46**(1): 9-21 (2011).
4. Taghipour S., Kananian A., Harlov D. and Oberhänsli R. Kiruna-type iron oxide-apatite deposits, Bafq district, Central Iran: Fluid-aided genesis of fluorapatite-monazite-xenotime assemblages. *Can. Mineral.* **53**(3): 479-496 (2015).
5. Bonyadi Z., Davidson G.J., Mehrabi B., Meffre S. and Ghazban F. Significance of apatite REE depletion and monazite inclusions in the brecciated Se–Chahun iron oxide–apatite deposit, Bafq district, Iran: insights from paragenesis and geochemistry. *Chem. Geol.* **281**(3): 253-269 (2011).
6. Daya A.A. Application of median indicator kriging in the analysis of an iron mineralization. *Arab. J. Geosci.* **8**(1): 367-377 (2015).
7. Khoshnoodi K., Yazdi M., Behzadi M. and Gannadi-Maragheh M. Using of ASTER, ETM+ and Gamma Spectrometry Airborne Data to Find the Relationship Between the Distribution of Alkali Metasomatism and REE Mineralization in the Bafq Area, Central Iran. *J. Sci. I. R. Iran.* **27**(1): 65-77 (2016).
8. Orris G. J., Dunlap P., Wallis J. and Wynn J. Phosphate occurrence and potential in the region of Afghanistan, including parts of China, Iran, Pakistan, Tajikistan, Turkmenistan, and Uzbekistan (No. 2015-1121). *U.S. Geol. Survey.* (2015).
9. Mohseni S. and Aftabi A. Structural, textural, geochemical and isotopic signatures of synglaciogenic Neoproterozoic banded iron formations (BIFs) at Bafq mining district (BMD), Central Iran: The possible Ediacaran missing link of BIFs in Tethyan metallogeny. *Ore. Geol. Rev.* **71**: 215-236 (2015).
10. Samani B.A. Metallogeny of the Precambrian in Iran. *Precambrian. Res.* **39**: 85-106 (1998a).
11. Samani B.A. Metallogenesis of apatite deposits in Central Iran and their dual origin based on the time and place. The 20th Annual Meeting of Earth Sciences, *GSI.* (in Farsi) (2000).
12. Daliran F. REE geochemistry of Bafq apatites, Iran; implication for the genesis of Kiruna-type iron ores. In: Stanclly et al. (Eds.) *Mineral Deposits; Processes to Processing. Balkema, Rotterdam.* 631-634 (1999).
13. Daliran F. Kiruna-type iron oxide-apatite ores and ‘apatites’ of the Bafq district, Iran, with an emphasis on the REE geochemistry of their apatites. In: Porter, T. M. (Ed.), *Hydrothermal Iron Oxide Copper Gold and Related Deposits: A Global Perspective.*, 2. *PGC Publishing, Adelaide, Australia*, 303–320 (2002).
14. Daliran F., Stosch H.G. and Williams P. Multistage metasomatism and mineralization at hydrothermal Fe oxide-REE-apatite deposits and “apatites” of the Bafq District, Central-East Iran. In: Andrew CJ et al. (eds) *Digging Deeper. Proceedings of the 9th Biennial SGA Meeting Dublin 2007. Irish Assoc Econ Geol.* 1501–1504 (2007).
15. Daliran F., Stosch H.G. and Williams P.A. review of the Early Cambrian Magmatic and Metasomatic events and their bearing on the genesis of the Fe oxide-REE-apatite deposits (IOA) of the Bafq District, Iran. In: Williams, et al. (Eds.), *Smart Science for Exploration and Mining: Proceedings of the 10th Biennial SGA Meeting, Townsville, Australia* 17th–20th August (2009).
16. Daliran F., Stosch H.G., Williams P., Jamli H. and Dorri

- M.B. Early Cambrian Iron Oxide–Apatite-REE (U) deposits of the Bafq district, East-Central Iran. In: Corriveau, L., Mumin, H. (Eds.), *Exploring for Iron Oxide Copper–Gold Deposits: Canada and Global Analogues. Geol. Assoc. Canada, Short Course Notes*. **20**: 143–155 (2010).
17. Förster H. and Jafarzadeh A. The Bafq mining district in Central Iran: a highly mineralized Infracambrian volcanic field. *Econ. Geol.* **89**: 1697–1721 (1994).
 18. Torab F.M. Geochemistry and metallogeny of magnetite-apatite deposits of the Bafq Mining District, Central Iran. Faculty of Energy and Economic Sciences, Clausthal *University of Technology, Ph.D. Thesis*, 144 p. (2008).
 19. Nadimi A. Evolution of the Central Iranian basement. *J. Gondwana. Res.* **12**: 324–333 (2007).
 20. Ramezani J. and Tucker R. The Saghand region, central Iran: U-Pb geochronology, petrogenesis and implications for Gondwana Tectonics. *Am. J. Sci.* **303**(3): 622- 665 (2003).
 21. Moore F. and Modabberi S. Origin of Choghart iron oxide deposit, Bafq mining district, Central Iran: new isotopic and geochemical evidence. *J. Sci. I. R. Iran.* **14** (3): 259-270 (2003).
 22. Dare S.A., Barnes S.J. and Beaudoin G. Did the massive magnetite “lava flows” of El Laco (Chile) form by magmatic or hydrothermal processes? New constraints from magnetite composition by LA-ICP-MS. *Miner. Deposita.* **50**(5): 607-617 (2015).
 23. Heidarian H., Lentz D., Alirezaei S., Peighambari S. and Hall D. Using the chemical analysis of magnetite to constrain various stages in the formation and genesis of the Kiruna-type Chadormalu magnetite-apatite deposit, Bafq district, Central Iran. *Miner. Petrol.* 1-16 (2016).
 24. Torab F.M. and Lehmann B. Magnetite-apatite deposits of the Bafq district, Central Iran: apatite geochemistry and monazite geochronology. *Mineral. Mag.* **71**: 347-363 (2007).
 25. Dargahi S., Arvin M., Pan Y. and Babaei A. The Origin of Co-Magmatic Andesite Enclaves in the Rabor Miocene Pyroxene Andesites, SE Kerman, Iran: Insights from Textural and Mineralogical Composition. *J. Sci. I. R. Iran.* **23**(4): 319-335 (2012).
 26. Wilkinson, Jamie J., Zhaoshan Chang, David R. Cooke, Michael J. Baker, Clara C. Wilkinson, Shaun Inglis, Huayong Chen, and J. Bruce Gemmel. The chlorite proximator: A new tool for detecting porphyry ore deposits. *J. Geochem. Explor.* **152**: 10-26 (2015).
 27. Eslamizadeh A. and Akbarian N. Mineralogy and Classification of Altered Host Rocks in the Zaghia Iron Oxide Deposit, East of Bafq, Central Iran. World Academy of Science, Engineering and Technology, International Science Index, Geological and Environmental Engineering, *WASET. Publ.* **17**(4): 2673-2677 (2015).
 28. Le Bas M.J., Le Maitre R.W., Streckeisen A. and Zanettin B. A chemical classification of volcanic rocks based on the total alkali-silica diagram. *J. Petrol.* **27**(3): 745-750 (1986).
 29. Irvine T. and Baragar W. A guide to the chemical classification of the common volcanic rocks. *Can. J. Earth. Sci.* **8**(5): 523-548 (1971).
 30. Winchester J.A. and Floyd P.A. Geochemical discrimination of different magma series and their differentiation products using immobile elements. *Chem. Geol.* **20**: 325-343 (1977).
 31. Hastie A.R., Kerr A.C., Pearce J.A. and Mitchell S.F. Classification of altered volcanic island arc rocks using immobile trace elements: development of the Th–Co discrimination diagram. *J. Petrol.* **48**(12): 2341-2357 (2007).
 32. Renjith M.L., Santosh M., Tang Li.M., Satyanarayanan M.M., Korakoppa T., Tsunogae D.V., Subba Rao A., Kesav Krishna and Nirmal Charan S. Zircon U–Pb age, Lu–Hf isotope, mineral chemistry and geochemistry of Sundamalai peralkaline pluton from the Salem Block, southern India: Implications for Cryogenian adakite-like magmatism in an aborted-rift. *J. Asian. Earth. Sci.* **115**: 321-344 (2016).
 33. Weaver B.L. and Tarney J. Empirical approach to estimating the composition of the continental crust. *Nature.* **310**: 575 - 577 (1984).
 34. Gill J. Orogenic andesites and plate tectonics. *Springer Science and Business Media.* **16**: (2012).
 35. El-Bialy M.Z. On the Pan-African transition of the Arabian–Nubian Shield from compression to extension: the post-collision Dokhan volcanic suite of Kid-Malhak region, Sinai, Egypt. *Gondwana. Res.* **17**(1): 26-43 (2010).
 36. Blundy J.D. and Wood B.J. Crystal-chemical controls on the partitioning of Sr and Ba between plagioclase feldspar, silicate melts, and hydrothermal solutions. *Geochim. Cosmochim. Ac.* **55**(1): 193-209 (1991).
 37. Sarifakioglu E., Dilek Y. and Sevin M. Jurassic–Paleogene intra-oceanic magmatic evolution of the Ankara Mélange, North-Central Anatolia, Turkey. *S.E. Discussions.* **5**(2): 1941-2004 (2013).
 38. McDonough W.F. and Sun S.S. The Composition of the Earth. *Chem. Geol.* **120**: 223-253(1995).
 39. Pålsson B.I., Martinsson O., Wanhainen C. and Frederiksson A. Unlocking rare earth elements from European apatite-iron ores. In *Proceedings 1st European Rare Earth Resources Conference ERES*. 211-220 (2014).
 40. Niktabar S.M., Moradian A., Ahmadipour H., Santos J. F. and Mendes, M. H. Petrogenesis of the Lalezar granitoid intrusions (Kerman Province - Iran). *J. Sci. I. R. Iran.* **26**(4): 333 - 348 (2015).
 41. Imchen W., Patil S.K., Rino V., Thong G.T., Pongen T.

- and Rao B.V. Geochemistry, petrography and rock magnetism of the basalts of Phek district, Nagaland. *Curr. Sci. India*. **108** (12): 2240 (2015).
42. Ohba T., Kimura Y. and Fujimaki H. High-magnesian andesite produced by two-stage magma mixing: a case study from Hachimantai, Northern Hanshu. *J. Petrol.* **48**: 627-465 (2007).
43. Taylors R. and McLennan S.M. The geochemical evolution of the continental crust. *Reviews of Geophysics* **33.2**: 241-265(1995).